5. S. P. A. Foder *et al.*, *Science* **251**, 767 (1991).
6. M. Schena *et al.*, *Proc. Natl. Acad. Sci. U.S.A.* **93**, 10614 (1996).
7. D. V. Nicolau, T. Tauguchi, H. Taniguchi, S. Yoshikawa, *Langmuir* **14**, 1927 (1998).
8. M. Mrksich *et al.*, *Proc. Natl. Acad. Sci. U.S.A.* **93**, 10775 (1996).
9. A. A. Bergman *et al.*, *Langmuir* **14**, 6785 (1998).
10. M. E. Browning-Kelley, K. Waud-Mesthrige, V. Hari, G.-Y. Liu, *Langmuir* **13**, 343 (1997).
11. K. Waud-Mesthrige, S. Xu, N. A. Amro, G.-Y. Liu, *Langmuir* **15**, 8580 (1999).
12. K. Waud-Mesthrige *et al.*, *Biophys. J.* **80**, 1891 (2001).
13. J. R. Kenseth, J. A. Harnisch, V. W. Jones, M. D. Porter, *Langmuir* **17**, 4105 (2001).
14. D. L. Wilson *et al.*, *Proc. Natl. Acad. Sci. U.S.A.* **98**, 13660 (2001).
15. K. L. Prime, G. M. Whitesides, *Science* **252**, 1164 (1991).
16. G. P. Lopez *et al.*, *J. Am. Chem. Soc.* **115**, 10774 (1993).
17. C. C. F. Blake *et al.*, *Nature* **206**, 757 (1965).
18. All DPN patterning and contact mode imaging experiments were done with a ThermoMicroscopes CP AFM interfaced with customized software and conventional Si_3N_4 cantilevers (Thermo Microscopes sharpened Microlever A, force constant = 0.05 N/m). Tapping mode images were taken with a Nanoscope IIIa and MultiMode microscope from Digital Instruments. Unless otherwise mentioned, all DPN patterning experiments were conducted at 40% relative humidity and 24°C with a tip-substrate contact force of 0.5 nN. A 90-μm scanner, with closed-loop scan control, was used for all DPN experiments to minimize piezo tube drift and alignment problems. Finally, attempts to use bovine serum albumin (BSA) as a passivation agent, instead of 11-mercaptoundecyltri(ethylene glycol), proved inferior and led to substrates with significant nonspecific binding of both proteins.
19. Supplementary material is available on *Science* Online at www.sciencemag.org/cgi/content/full/1067172/DC1.
20. E. W. Silverton, M. A. Navia, D. R. Davies, *Proc. Natl. Acad. Sci. U.S.A.* **74**, 5140 (1977).
21. The basic structure of monomeric IgG consists of two identical halves; each half comprises a heavy and a light chain. The heavy chains form the base of the "Y" and are COOH-terminated, and the light chains form the arms of the "Y" and are NH_2-terminated. Hence, the data is consistent with the arms of the "Y" interacting with the MHA nanofeatures and the anti-IgG complexing to the exposed base of the "Y."
22. F. Kimizuka *et al.*, *J. Biochem.* **110**, 284 (1991).
23. J. C. Adams, *Cell. Mol. Life Sci.* **58**, 371 (2001).
24. These arrays were passivated with 11-mercaptoundecyl-tri(ethylene glycol), and then modified with Retronectin by placing a 50-μl droplet of the protein (50 μg/ml) dissolved in PBS solution on the patterned surface for 30 min. The substrate was then repeatedly rinsed with PBS and NANOpure water.
25. R. D. Piner, J. Zhu, F. Xu, S. Hong, C. A. Mirkin, *Science* **283**, 661 (1999).
26. S. Hong, J. Zhu, C. A. Mirkin, *Science* **286**, 523 (1999).
27. S. Hong, C. A. Mirkin, *Science* **288**, 1808 (2000).
28. C.A.M. acknowledges the Air Force Office of Scientific Research, the Defense Advanced Research Projects Agency (DARPA), and the NSF for support of this research. J.C.S. and M.M. acknowledge DARPA and NIH for generous support.

16 October 2001; accepted 28 January 2002
Published online 7 February 2002;
10.1126/science.1067172
Include this information when citing this paper.

Niobium-Zirconium Chronometry and Early Solar System Development

Maria Schönbächler,[1]* Mark Rehkämper,[1] Alex N. Halliday,[1] Der-Chuen Lee,[1] Michèle Bourot-Denise,[3] Brigitte Zanda,[3,4] Bodo Hattendorf,[2] Detlef Günther[2]

Niobium-92 (^{92}Nb) decays to zirconium-92 (^{92}Zr) with a half-life of 36 million years and can be used to place constraints on the site of *p*-process nucleosynthesis and the timing of early solar system processes. Recent results have suggested that the initial ^{92}Nb/^{93}Nb of the solar system was high ($>10^{-3}$). We report Nb-Zr internal isochrons for the ordinary chondrite Estacado (H6) and a clast of the mesosiderite Vaca Muerta, both of which define an initial ^{92}Nb/^{93}Nb ratio of $\sim10^{-5}$. Therefore, the solar system appears to have started with a ratio of $<3 \times 10^{-5}$, which implies that Earth's initial differentiation need not have been as protracted as recently suggested.

Some extinct radionuclides were sufficiently abundant at the start of the solar system that they produced variations in the abundance of their daughter isotopes in early-formed objects (*1*). Such nuclides provide information about late-stage presolar nucleosynthetic sites and the time scales over which the early solar system formed and first differentiated (*2–4*). Of considerable interest in this regard is ^{92}Nb, which decays by electron capture with a half-life of 36 ± 3 million years (My) to ^{92}Zr (*5, 6*). ^{92}Nb is a shielded nuclide that forms by the *p*-process only. The *p*-process is a nucleosynthetic process that occurs in supernovae and produces proton-rich nuclides. Therefore, the initial abundance of ^{92}Nb provides information on stellar nucleosynthesis before the start of the solar system.

Both Nb and Zr are refractory and lithophile, except under reducing conditions when Nb may become siderophile (*7*). Within the Earth the dominant Nb/Zr fractionation mechanisms are silicate partial melting (*8*) and the crystallization of accessory minerals such as zircon, ilmenite, and rutile. The Zr isotopic compositions of early reservoirs can therefore vary in response to early differentiation processes and can help in dating planetary differentiation, if the initial abundance of ^{92}Nb (or ^{92}Nb/^{93}Nb) was sufficiently high.

Early results demonstrated that the initial ^{92}Nb/^{93}Nb of the solar system was <0.007 (*9*). Evidence of formerly live ^{92}Nb was first identified in a Nb-rich rutile from the iron meteorite Toluca (*10*). An initial ^{92}Nb/^{93}Nb of 1.6 (±0.3) $\times$ 10^{-5} was inferred. More recently, three studies using a multiple-collector inductively coupled plasma mass spectrometer (MC-ICPMS) proposed that the initial ^{92}Nb/^{93}Nb ratio of the solar system was higher by two orders of magnitude ($\sim10^{-3}$) (*11–13*). Such a high value limits the possible sites for *p*-process nucleosynthesis and places specific constraints on the time scales for the development of differentiated reservoirs on the Earth and Moon. For example, it has been argued that large silicate reservoirs in the Earth and Moon formed >50 My after the start of the solar system (*12*). However, such a result requires that the Toluca rutile grew very late (>200 My). In contrast, a combined Zr isotopic and U-Pb age study of an early zircon from a eucrite implied that the initial ^{92}Nb/^{93}Nb ratio was $<10^{-4}$ (*14*).

Here, we used the internal isochron approach to determine the initial ^{92}Nb/^{93}Nb ratio of the solar system. Two meteorites were studied in which ilmenite with high Nb/Zr is in textural equilibrium with other phases having intermediate Nb/Zr. Because the half-life of ^{92}Nb is long (36 My) and the level of uncertainty concerning the initial solar system abundance is more than two orders of magnitude, the critical concern is not the exact age of the meteorite (provided it is reasonably early) but the acquisition of a reliable isochron from a cogenetic suite of phases that remained undisturbed after their formation. Therefore, we used the equilibrated but only weakly shocked (S1) H6 ordinary chondrite Estacado, which has a single generation of ilmenite, and a eucritic clast from the mesosiderite Vaca Muerta.

Using a Nu Plasma MC-ICPMS, we were able to measure ε^{92}Zr with an external precision of ±0.3 ε units (2σ standard deviation) for samples with only 50 ng of Zr (*15*). The Nb/Zr ratios were determined by inductively coupled plasma dynamic reaction cell mass

[1]Institute of Isotope Geology and Mineral Resources, [2]Laboratory of Inorganic Chemistry, ETH Zürich, 8092 Zürich, Switzerland. [3]Museum national d'Histoire naturelle, 75005, Paris, France. [4]Rutgers University, Department of Geological Sciences, Wright Lab, Piscataway, NJ 08854-8066, USA.

*To whom correspondence should be addressed. E-mail: maria@erdw.ethz.ch

spectrometry (ICP-DRCMS) without chemical separation (*15, 16*).

To check for terrestrial Zr isotope anomalies and test our ability to measure the isotopic composition of Zr extracted from different matrices, we analyzed 12 early zircons [aliquots of those described by (*17*)], two basalts and a rhyolite (from Iceland), a lherzolite (Cameroon Line), and ilmenite (from Russia) (*15*). The analyzed zircons have ages of up to 4100 Ma (million years ago) (*17*) and are among the oldest terrestrial minerals. Variations in the Zr isotopic composition of old rocks or minerals are expected only if the initial ^{92}Nb abundance is extremely high. For a solar system initial ^{92}Nb/^{93}Nb ratio of $\sim 10^{-5}$, there will be no detectable Zr isotopic effects even in the oldest terrestrial zircons. Earlier studies (*12, 14, 18*) reached differing conclusions regarding the homogeneity of terrestrial Zr. However, our ^{92}Zr/^{90}Zr, ^{91}Zr/^{90}Zr, and ^{96}Zr/^{90}Zr ratios for terrestrial samples are identical with the value obtained for a standard solution of National Institute Standards and Technology Standard Reference Material 3169 Zr and do not indicate any variation in the Zr composition of Earth (*15*). This implies a homogenous distribution of Zr isotopes for the bulk silicate Earth.

The mineral fractions (*15*) and whole-rock data for Estacado and the Vaca Muerta clast both define isochrons, but with limited variation in ^{92}Zr/^{90}Zr (Fig. 1). The Estacado whole-rock sample and the mineral fractions of olivine/pyroxene and chromite all agree with the terrestrial Zr isotopic composition within analytical uncertainty. However, the ilmenite with a Nb/Zr ratio 20 times that of chondritic ($\sim$0.065) yields an ε^{92}Zr of +1.0 ± 0.4. The results for Vaca Muerta are similar (Table 1). The slope of the regression line defines an initial ^{92}Nb/^{93}Nb at the time of closure of 1.2 (±0.6) × 10^{-5} for Estacado (Fig. 1A) and 0.6 (±0.3) × 10^{-5} for Vaca Muerta (Fig. 1B). These values are effectively identical to the Toluca results (*10*) and are consistent with the zircon data for the Camel Donga eucrite (*14*).

A high initial ^{92}Nb/^{93}Nb on the order of 10^{-3} was obtained for specific calcium-aluminum-rich inclusions (CAI) from Allende (*12, 13*). The CAIs are believed to be among the earliest objects that formed in the solar system (*19*). The production rate of cosmogenic ^{92}Zr is too small to generate significant variations in the calculated initial ^{92}Nb/^{93}Nb ratios (*20*). Both ^{92}Zr and ^{96}Zr isotope anomalies have been reported for CAIs (*13*). Therefore, the possibility remains that CAIs preserve a component with a presolar Zr isotope signature, analogous to those reported for presolar graphite grains (*21*). A heterogeneous distribution of ^{92}Nb in the early solar system could also cause different estimates of the initial abundance of ^{92}Nb. This would require a variability in the initial ^{92}Nb/^{93}Nb between 10^{-3} and 10^{-5} and should produce measurable ^{92}Zr anomalies in whole-rock meteorites. However, the observed ^{92}Zr isotopic variations in bulk chondrites (*13*) have not been yet confirmed (*12, 22*). This indicates that further work is needed to confirm and understand these reported ^{92}Zr anomalies.

One way to reconcile the various results is resetting or slow cooling (>200 My) of the samples yielding low values: Toluca, Vaca Muerta, Camel Donga, and Estacado. This is inconsistent with a considerable amount of independent age data. Estacado (H6) yields a K-Ar age (4450 Ma) only 30 My younger than Kernouvé (another H6 chondrite) (*23*), which is likely to have experienced the same events as all H6 chondrites. The Pb-Pb age of phosphates extracted from Kernouvé (H6) and Guarena (H6) indicate that these meteorites underwent a metamorphic event or cooling around 45 My and 61 My, respectively, after the formation of the Allende CAIs (*19*). The H6 chondrites are, therefore, early objects and their equilibrated textures cannot be of late origin. The Sm-Nd chronology of Vaca Muerta clasts (*24*) and the U-Th-Pb systematics of Vaca Muerta zircons (*25*) yield similar ages of 4480 ± 190 Ma and

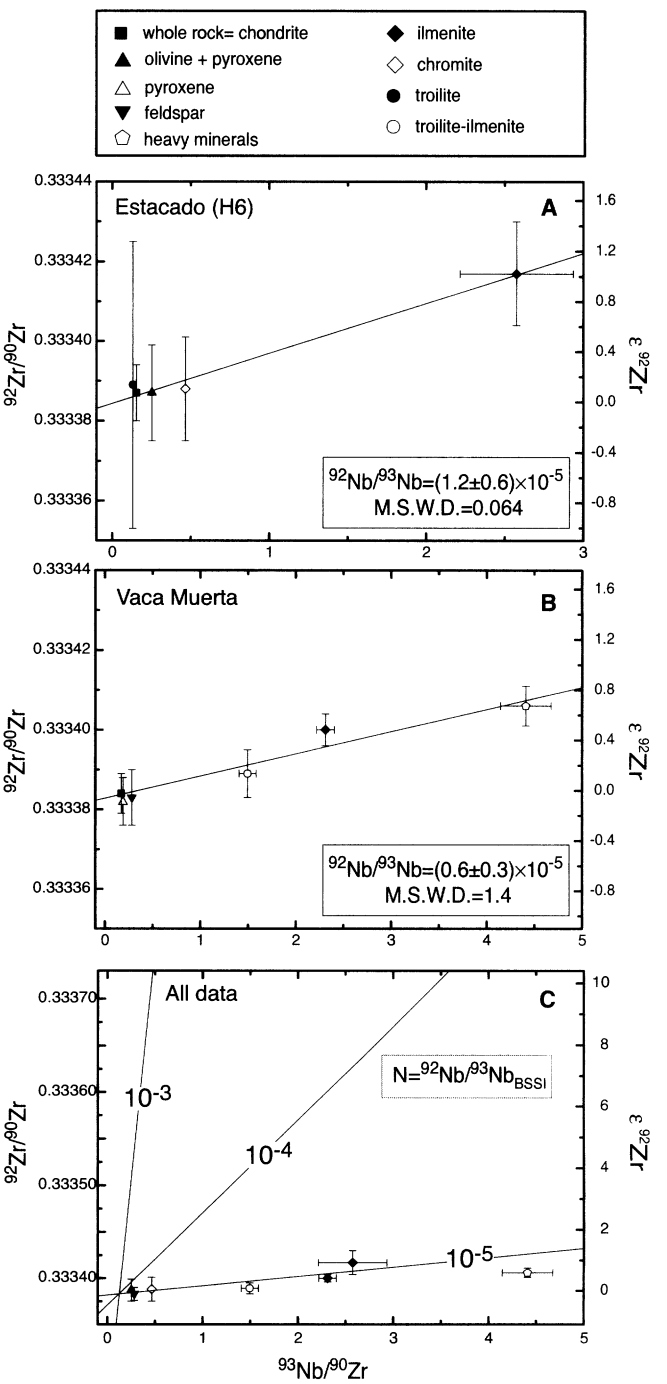

Fig. 1. Nb-Zr isochron diagrams for (**A**) Estacado (H6) and (**B**) a clast of the mesosiderite Vaca Muerta. Only the ilmenite and heavy mineral fractions show a ^{92}Zr anomaly outside our analytical error of ±0.3 ε^{92}Zr (*15*). The initial ^{92}Zr/^{90}Zr ratios of the isochrons (0.333384 ± 6 and 0.333382 ± 3 for Estacado and Vaca Muerta, respectively; errors refer to the least significant digits) overlap with the terrestrial value. (**C**) The strong constraints that the Estacado and Vaca Muerta data provide on an initial ^{92}Nb/^{93}Nb close to 10^{-5}. All data points for Estacado and Vaca Muerta with a Nb/Zr ratio greater than chondritic are plotted. Error bars reflect the $2\sigma_{mean}$ internal run precision. BSSI, bulk solar system initial.

4563 ± 15 Ma, respectively.

To provide more direct time constraints, we have acquired Hf-W isotope data for some of the Estacado and Vaca Muerta mineral separates (*15*). ^{182}Hf (half-life = 9 My) decays to ^{182}W such that W isotopic variations can only be produced within the first 50 My of the solar system. Small excesses of ^{182}W have previously been detected in Vaca Muerta zircons (*26*). We find large W isotopic variations among the aliquots that we have analyzed for Zr (*15*). Sulfide equilibrates readily, yet the two troilite fractions of Estacado display negative εW values of –2.46 ± 0.47 and –2.05 ± 0.56, indicating that the latest time of sulfide/silicate equilibration was 9 ± 3 My and 11 ± 4 My, respectively, after the origin of the solar system, assuming that the initial ^{182}Hf/^{180}Hf was 2.4×10^{-4}. The W isotopic compositions and Hf/W ratios for the Vaca Muerta pyroxene and feldspar separates (*15*) define a ^{182}Hf/^{180}Hf of 7.68 (±0.8) $\times 10^{-5}$. Therefore, these phases appear to have last equilibrated 14.8 ± 1.3 My after the start of the solar system. Even if this error is increased somewhat to allow for systematic Hf-W uncertainties, there is little doubt that Estacado and Vaca Muerta last underwent internal W isotope equilibration within the first 20 My of solar system history. Therefore, the apparent discrepancy with other recently published Nb-Zr data cannot be explained easily by later equilibration. The Estacado initial ^{92}Nb/^{93}Nb of 1.2 (±0.6) $\times 10^{-5}$ should be very close to the solar system initial abundance within a factor of 2 (Fig. 2). The slightly lower initial ^{92}Nb/^{93}Nb of Vaca Muerta is consistent with the Hf-W evidence for a later closure of the phases in the mesosiderite relative to Estacado. However, both initial ^{92}Nb/^{93}Nb values are identical within the analytical errors, consistent with independent evidence for early planetesimal differentiation (*27, 28*).

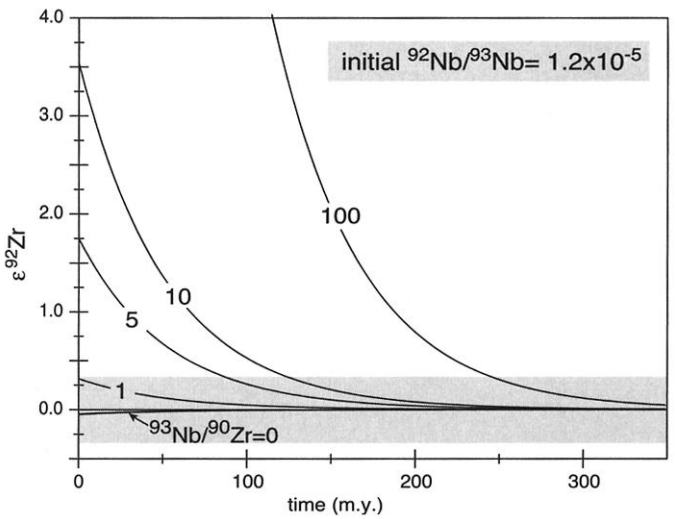

Fig. 2. Variation in ε^{92}Zr versus time, starting with the formation of the solar system and assuming a ^{92}Nb/^{93}Nb of 1.2×10^{-5} for a ^{93}Nb/^{90}Zr ratio up to 100. The shaded area shows the external reproducibility for terrestrial standards. The numbers on the curves denote different ^{93}Nb/^{90}Zr ratios (chondritic ^{93}Nb/^{90}Zr ratio = ~0.127).

With a low initial ^{92}Nb/^{93}Nb ratio of $\sim 10^{-5}$, the timing of terrestrial core formation, the growth rate of Hadean continents, and the longevity of the lunar magma ocean (*12, 29, 30*) can now be considered to be underconstrained from Nb-Zr systematics (Fig. 2).

The low initial abundance of ^{92}Nb also reopens the range of possibilities that can be considered for *p*-process nucleosynthesis. As a *p*-only nuclide, ^{92}Nb is predominantly produced in supernovae by photodisintegration (*31*). The modeling of other processes such as spallation synthesis (*10, 31, 32*) shows that these can be only a minor contributor in the synthesis of *p*-nuclei because they fail to explain the solar abundance pattern. The calculated production ratios for ^{92}Nb/^{93}Nb, as predicted by several models for Type Ia and Type II supernovae (*33–36*), are in the range of 2.1×10^{-3} to 9.2×10^{-3}. Only one Type II model (*11, 37*) yields a higher production ratio of 0.35, and is able to explain the high abundance of stable *p*-process ^{92}Mo in the solar system. However, it is inconsistent with the data presented here.

The range 2.1×10^{-3} to 9.2×10^{-3}, in contrast, is in good agreement with our results. To deduce the abundance of ^{92}Nb at the time of the formation of the solar system from this range, it is important to consider two factors: (i) the free decay time interval between the last nucleosynthesis and the formation of the solar system, and (ii) the amount of ^{92}Nb at the start of this interval, which is a function of the duration of nucleosynthesis. The 36-My half-life of ^{92}Nb enables the use of an averaging model (*38*), which includes continuous nucleosynthesis at a constant rate (*39, 40*). Assuming a 10,000-My period of nucleosynthesis, such a model predicts that 0.5% of the total ^{92}Nb produced is present at the end of nucleosynthesis. This factor applied to the calculated produc-

Table 1. Zr isotopic data and Nb and Zr concentration data. $\varepsilon^{9x}Zr = \{[(^{9x}Zr/^{90}Zr)_{meas} - (^{9x}Zr/^{90}Zr)_{std}]/(^{9x}Zr/^{90}Zr)_{std}\} \times 10^4$, with $(^{9x}Zr/^{90}Zr)_{std} = 0.333383$ for ^{92}Zr/^{90}Zr, 0.217930 for ^{91}Zr/^{90}Zr, and 0.054372 for ^{96}Zr/^{90}Zr. The quoted analytical uncertainties for the Zr isotopic compositions and εZr values reflect the internal ($2\sigma_{mean}$) within-run precision. The errors of ^{92}Zr/^{90}Zr refer to the least significant digits only. The εZr values do not include uncertainties for the standard. The 2σ long-term external reproducibilities, based on multiple measurements of the standard over a period of more than a year, are 0.3, 0.4, and 1.2 ε units for ^{92}Zr/^{90}Zr, ^{91}Zr/^{90}Zr, and ^{96}Zr/^{90}Zr, respectively (*15*).

Sample	Nb (ppm)	Zr (ppm)	^{93}Nb/^{90}Zr ±2σ mean	^{92}Zr/^{90}Zr ±2σ mean	ε^{92}Zr ±2σ mean	ε^{91}Zr ±2σ mean	ε^{96}Zr ±2σ mean
			Estacado				
Olivine + pyroxene	0.47	3.6	0.253 ± 0.020	0.333387 ± 12	0.13 ± 0.35	−0.59 ± 0.66	
Ilmenite	83	58	2.58 ± 0.36	0.333417 ± 13	1.01 ± 0.38	0.11 ± 0.38	1.73 ± 1.12
Whole rock	0.51	6.4	0.154 ± 0.008	0.333387 ± 07	0.11 ± 0.22	0.12 ± 0.26	0.27 ± 0.90
Chromite	0.29	1.2	0.466 ± 0.004	0.333388 ± 13	0.15 ± 0.39		0.75 ± 1.41
Troilite (fraction a)	0.057	0.83	0.132 ± 0.018	0.333389 ± 36	0.17 ± 1.08	−1.37 ± 1.00	
			Vaca Muerta				
Ilmenite/troilite	56	73	1.50 ± 0.09	0.333389 ± 6	0.19 ± 0.18	−0.19 ± 0.17	0.67 ± 0.45
Whole rock	3.9	43	0.173 ± 0.004	0.333384 ± 5	0.02 ± 0.16	−0.14 ± 0.16	0.10 ± 0.36
Feldspar	0.64	4.3	0.284 ± 0.012	0.333383 ± 7	0.00 ± 0.20	−0.19 ± 0.13	0.70 ± 0.45
Pyroxene	2.5	26	0.190 ± 0.012	0.333382 ± 6	−0.04 ± 0.18	−0.09 ± 0.12	0.10 ± 0.42
Ilmenite	249	208	2.31 ± 0.09	0.333400 ± 4	0.52 ± 0.11	−0.05 ± 0.12	0.42 ± 0.26
Heavy minerals	41	18	4.41 ± 0.27	0.333406 ± 5	0.69 ± 0.15	−0.07 ± 0.13	0.65 ± 0.47

tion ratios (*33–36*) yields an initial $^{92}Nb/^{93}Nb$ for the solar system of 1×10^{-5} to 4.6×10^{-5}, if the free decay interval is not considered. Our estimate based on Estacado falls into this range. Taking into account the free decay interval [up to 50 My (*10*)] may further lower the calculated value by a factor of 2 or more. Nonetheless, most production ratio yields of different supernova models (type Ia and type II) are quite similar to our measured value of $1.2 (\pm 0.6) \times 10^{-5}$. Thus, our data provide only limited constraints on the type of supernova that produced the ^{92}Nb initially present in the solar system.

References and Notes

1. F. A. Podosek, T. D. Swindle, in *Meteorites and the Early Solar System*, J. F. Kerridge, M. S. Matthews, Eds. (Univ. of Arizona Press, Tucson, AZ, 1988), pp. 1093–1113.
2. G. J. Wasserburg, in *Protostars and Planets II*, D. C. Black, M. S. Matthews, Eds. (Univ. of Arizona Press, Tucson, AZ, 1985), pp. 703–737.
3. T. D. Swindle, in *Protostars and Planets III*, E. H. Levy, J. I. Lunine, Eds. (Univ. of Arizona Press, Tucson, AZ, 1993), pp. 867–881.
4. F. A. Podosek, R. H. Nichols, in *Astrophysical Implications of the Laboratory Study of Presolar Materials*, T. J. Bernatowicz, E. Zinner, Eds. (API, New York, 1997), pp. 617–647.
5. T. Makino, M. Honda, *Geochim. Cosmochim. Acta* **46**, 565 (1982).
6. D. R. Nethaway, A. L. Prindle, R. A. Van Konyenburg, *Phys. Rev. C* **17**, 1409 (1978).
7. J. Wade, B. J. Wood, *Nature* **409**, 75 (2001).
8. K. P. Jochum, H. M. Seufert, B. Spettel, H. Palme, *Geochim. Cosmochim. Acta* **50**, 1173 (1986).
9. J. F. Minster, C. J. Allègre, *Geochim. Cosmochim. Acta* **46**, 565 (1982).
10. C. L. Harper Jr., *Astrophys. J.* **466**, 437 (1996).
11. Q. Z. Yin *et al.*, *Astrophys. J.* **535**, L49 (2000).
12. C. Muenker *et al.*, *Science* **289**, 1538 (2000).
13. C. Sanloup, J. Blichert-Toft, P. Trélouk, P. Gillet, F. Albarède, *Earth Planet. Sci. Lett.* **184**, 75 (2000).
14. T. Hirata, *Chem. Geol.* **176**, 323 (2001).
15. Details of analytical methods and supplementary data are available on *Science* Online at www.sciencemag.org/cgi/content/full/295/5560/1705/DC1.
16. B. Hattendorf, D. Günther, M. Schönbächler, A. N. Halliday, *Anal. Chem.* **73**, 5494 (2001).
17. Y. Amelin, D. C. Lee, A. N. Halliday, R. T. Pidgeon, *Nature* **399**, 252 (1999).
18. S. K. Sahoo, A. Masuda, *Chem. Geol.* **141**, 117 (1997).
19. C. Göpel, G. Manhes, C. J. Allègre, *Earth Planet. Sci. Lett.* **121**, 153 (1994).
20. I. Leya, R. Wieler, A. N. Halliday, *Lunar Planet. Sci. Conf.* **XXXII**, 1521 (2001).
21. K. Nicolussi *et al.*, *Astrophys. J.* **504**, 492 (1998).
22. M. Schönbächler *et al.*, *Meteorit. Planet Sci.* **36**, A184 (2001).
23. I. Flohs, *Eos* **62**, 17 (1981).
24. B. W. Stewart, D. A. Papanastassiou, G. J. Wasserburg, *Geochim. Cosmochim. Acta* **58**, 3487 (1994).
25. T. R. Ireland, F. Wlotzka, *Earth Planet. Sci. Lett.* **109**, 1 (1992).
26. T. R. Ireland, *Lunar Planet. Sci. Conf. XXXII* **22**, 609 (1991).
27. G. W. Lugmair, A. Shukolyukov, *Geochim. Cosmochim. Acta* **62**, 2863 (1998).
28. D. C. Lee, A. N. Halliday, *Nature* **388**, 854 (1997).
29. S. B. Jacobsen, Q. Z. Yin, *Lun. Planet. Sci. Conf.* **XXXII**, abstract 1961 (2001).
30. Q. Z. Yin, S. B. Jacobsen, J. Blichert-Toft, P. Télouk, F. Albarède, *Lunar Planet. Sci. Conf.* **XXXII**, abstract 2128 (2001).
31. D. L. Lambert, *Astron. Astrophys. Rev.* **3**, 201 (1992).
32. D. D. Clayton, E. Dwek, S. E. Woosley, *Astrophys. J.* **214**, 300 (1977).
33. S. E. Woosley, W. M. Howard, *Astrophys. J. Suppl. Ser.* **36**, 285 (1978).
34. W. M. Howard, B. S. Meyer, S. E. Woosley, *Astrophys. J.* **373**, L5 (1991).
35. W. M. Howard, B. S. Meyer, in *Nuclei in the Cosmos II*, F. Käppeler, K. Wisshak, Eds. (IOP, London, 1993), pp. 575–580.
36. M. Rayet *et al.*, *Astron. Astrophys.* **298**, 517 (1995).
37. R. D. Hoffman, S. E. Woosley, G. M. Fuller, B. S. Meyer, *Astrophys. J.* **460**, 478 (1996).
38. A. G. W. Cameron, in *Protostars and Planets III*, E. H. Levy, J. I. Lunine, Eds. (Univ. of Arizona Press, Tucson, AZ, 1993), pp. 47–73.
39. G. J. Wasserburg, W. A. Fowler, F. Hoyle, *Phys. Rev. Lett.* **4**, 112 (1960).
40. A. G. W. Cameron, *Icarus* **1**, 13 (1962).

41. We thank three anonymous reviewers for their helpful comments, the Museum of Natural History in Paris for provision of the sample of Estacado, R. Hewins for the sample of Vaca Muerta, and Y. Amelin for the terrestrial zircon samples. Supported by Swiss National Fonds and ETH.

22 October 2001; accepted 23 January 2002

Imaging Sites of Receptor Dephosphorylation by PTP1B on the Surface of the Endoplasmic Reticulum

Fawaz G. Haj,[1] Peter J. Verveer,[2] Anthony Squire,[2] Benjamin G. Neel,[1]* Philippe I. H. Bastiaens[2]*

When bound by extracellular ligands, receptor tyrosine kinases (RTKs) on the cell surface transmit critical signals to the cell interior. Although signal termination is less well understood, protein tyrosine phosphatase–1B (PTP1B) is implicated in the dephosphorylation and inactivation of several RTKs. However, PTP1B resides on the cytoplasmic surface of the endoplasmic reticulum (ER), so how and when it accesses RTKs has been unclear. Using fluorescence resonance energy transfer (FRET) methods, we monitored interactions between the epidermal- and platelet-derived growth factor receptors and PTP1B. PTP1B-catalyzed dephosphorylation required endocytosis of the receptors and occurred at specific sites on the surface of the ER. Most of the RTKs activated at the cell surface showed interaction with PTP1B after internalization, establishing that RTK activation and inactivation are spatially and temporally partitioned within cells.

Most peptide growth factors signal through receptor tyrosine kinases (RTKs). Growth factor binding promotes oligomerization of receptors at the plasma membrane, which leads to receptor activation and the phosphorylation of multiple receptor tyrosyl residues. These tyrosyl phosphorylation sites recruit proteins with Src homology 2 and phosphotyrosine-binding domains, thereby assembling multiprotein complexes that propagate the signal. The amount of phosphotyrosine on RTKs, and thus their signaling capacity, is determined by the balance between RTK activity and the activities of specific protein-tyrosine phosphatases (PTPs). Several PTPs have been implicated in RTK dephosphorylation, but exactly how, when, and where RTK inactivation takes place has remained unknown.

To address the spatiotemporal regulation of RTK dephosphorylation, we investigated the interaction between PTP1B and two RTKs, the epidermal growth factor receptor (EGFR) and the platelet-derived growth factor receptor–β (PDGFR). PTP1B is a widely expressed, prototypical nontransmembrane PTP that can dephosphorylate several RTKs, including the EGFR (*1*) and the insulin receptor (IR) (*2*). Indeed, PTP1B-deficient mice are hypersensitive to insulin and show enhanced tyrosyl phosphorylation of the IR in some insulin-responsive tissues (*3*, *4*). Although $PTP1B^{-/-}$ mice show no obvious evidence of increased EGFR or PDGFR signaling, primary and immortalized $PTP1B^{-/-}$ fibroblasts exhibit increased and sustained ligand-induced tyrosyl phosphorylation of the EGFR and PDGFR, indicating that PTP1B may be a biologically relevant EGFR and PDGFR phosphatase (*5*). However, PTP1B is localized exclusively on the cytoplasmic face of the endoplasmic reticulum (ER), by means of a hydrophobic COOH-terminal anchor sequence (*6*, *7*). These findings raise a conundrum: How does an ER-resident phosphatase dephosphorylate RTKs localized on the plasma membrane or in endocytic vesicles?

The steady-state population of complexes between wild-type PTP1B and RTKs is, on average, very low in cells, because PTP1B has a

[1]Cancer Biology Program, Division of Hematology-Oncology, Department of Medicine, Beth Israel–Deaconess Medical Center, Boston, MA 02115, USA. [2]European Molecular Biology Laboratory, Meyerhofstrasse 1, 69117 Heidelberg, Germany.

*To whom correspondence should be addressed. E-mail: bneel@caregroup.harvard.edu (B.G.N.), bastiaen@embl-heidelberg.de (P.I.H.B.)